Experimental and Computational Studies of the Phenyl Radical Reaction with Allene†

J. Park,* I. V. Tokmakov, and M. C. Lin

Department of Chemistry, Emory University, Atlanta, Georgia 30322

Received: January 31, 2007; In Final Form: February 23, 2007

The kinetics for the gas-phase reaction of phenyl radicals with allene has been measured by cavity ring-down spectrometry (CRDS), and the mechanism and initial product branching have been elucidated with the help of quantum-chemical calculations. The absolute rate constant measured by the CRDS technique can be expressed by the following Arrhenius equation: k_{allene} (T = 301 − 421 K) = (4.07 ± 0.38) × 10^{11} exp[−(1865 ± 85)/T] cm^3 mol^{-1} s^{-1}. Theoretical calculations, employing high level G2M energetic and IRCMax(RCCSD-(T)//B3LYP-DFT) molecular parameters, indicate that under our experimental conditions the most preferable reaction channel is the addition of phenyl radicals to the terminal carbon atoms in allene. Predicted total rate constants agree with the experimental values within 40%. Calculated total and branching rate constants are provided for high-T kinetic modeling.

I. Introduction

Gas-phase reactions of aryl radicals with unsaturated hydrocarbons play an important role in the molecular growth of polycyclic aromatic hydrocarbons (PAHs) and soot during hydrocarbon combustion and pyrolysis.[1−4] Similar processes are believed to be involved in PAH formation in the photospheres of carbon-rich stars.[5−7] A better understanding of the PAH formation mechanism requires the development of a comprehensive kinetic database for the elementary reactions of aryl radicals. In building this database, it is impossible to rely exclusively on the measured kinetic data due to the limitations of experimental techniques and a sheer volume of the elementary reactions involved. Instead, simple and effective computational tools should be used to estimate the vast majority of the required kinetic parameters from accurate experimental and theoretical results for a small subset of prototypical reactions, such as the reactions of the simplest aromatic radical, phenyl (C_6H_5), with small (C_2 and C_3) unsaturated hydrocarbons.

Our group has devoted considerable efforts to studying the gas-phase chemistry of phenyl, using available experimental tools, as well as accurate quantum-chemical and theoretical-kinetic calculations. The cavity ring-down spectrometry (CRDS) technique has been applied to measure the total rate constants of the C_6H_5 reactions with a number of species.[8] We have also employed high-level electronic structure calculations in combination with statistical Rice−Ramsperger−Kassel−Marcus (RRKM)/master equation kinetic modeling to provide detailed theoretical accounts of the mechanism and kinetics for important prototypical reactions of C_6H_5 with acetylene[9] and ethylene,[10] the simplest unsaturated hydrocarbons. Recently, we have brought together our experimental and theoretical methodologies to investigate the mechanism and kinetics for the reactions of C_6H_5 with propyne[11] and propene.[12] This article continues this series by contributing a direct experimental determination of the total rates and a theoretical investigation of the initial product branching for the reaction of C_6H_5 with allene (R1−R3), the simplest hydrocarbon with cumulative double bonds:

$$C_6H_5 + CH_2{=}C{=}CH_2 \rightarrow C_6H_5CH_2CCH_2\ [\mathbf{1}] \quad \text{(R1)}$$

$$\rightarrow C_6H_5C(CH_2)_2\ [\mathbf{2}] \quad \text{(R2)}$$

$$\rightarrow C_6H_6 + CH_2CCH \quad \text{(R3)}$$

The initial product branching (reactions R1−R3) results from taking into consideration three different sites (H, C-terminal, and C-central) of the phenyl radical attack on allene. The addition of C_6H_5 to the unsaturated carbon atoms yields 3-phenylpropen-2-yl [**1**] and 2-phenylpropen-2-yl [**2**] radicals with an excess of internal energy,[13] whereas the C_6H_5 attack on the H atom leads to the H-abstraction products (benzene and propargyl radical).

In fact, chemically activated radicals [**1**]* and [**2**]* may follow further isomerization and decomposition pathways on the global [C_9H_9] potential energy surface. These transformations may result in additional (secondary) product branching for the reaction of C_6H_5 with allene. Recently, a large part of the [C_9H_9] ground state PES has been explored by Vereecken and coworkers[14] at the B3LYP-DFT/6−311+G(d,p) level of theory. Additional single-point calculations were performed at the QCISD(T) and CCSD(T) levels with the 6−311G(d,p) basis set to obtain more accurate estimates of the entrance barriers, including the barriers of reactions R1−R3 (TS1−TS3). An extensive search of the PES revealed various isomerization pathways (most importantly, phenyl and H migrations and intramolecular cyclizations) and several exit channels which are readily accessible to the chemically activated intermediates [**1**]* and [**2**]* formed by the addition of C_6H_5 to allene (R1, R2). The role of these channels in the product distribution of the C_6H_5 + C_3H_4 (allene and propyne) reactions has been assessed in the theoretical-kinetic studies of Vereecken et al.[15,16] They found that the most important exit channels ultimately lead to indene and substituted acetylenes and allenes, including C_6H_5-CCH, $C_6H_5CCCH_3$, and $C_6H_5CH{=}C{=}CH_2$.

In this work, our main goal is to benchmark the calculated kinetic parameters against the experimental total rate constant.

† Part of the special issue "M. C. Lin Festschrift".

* Corresponding author. E-mail: jpark05@emory.edu. Phone: 404-727-2823.

10.1021/jp0708502 CCC: $37.00
Published on Web 04/14/2007

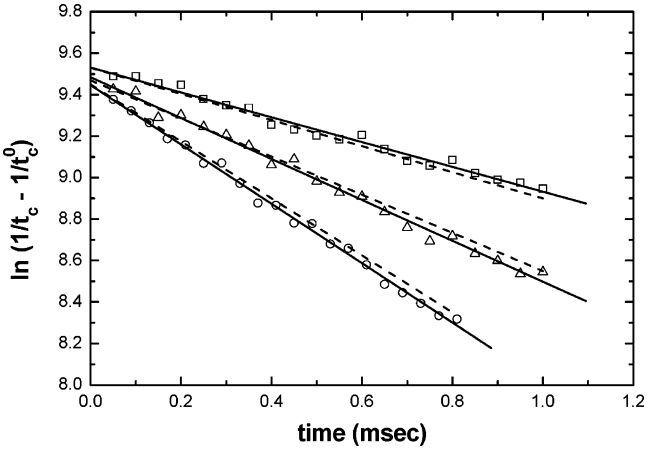

Figure 1. Typical pseudo-first-order decay plots for the reaction of C_6H_5 with allene. □, $[C_3H_4] = 0$, △, $[C_3H_4] = 3.52 \times 10^{-7}$ mol cm^{-3} at 301 K and, ○, $[C_3H_4] = 1.55 \times 10^{-7}$ mol cm^{-3} at 421 K. Dashed lines are kinetically modeled results using our predicted k_1 and initial conditions of $[C_6H_5]_0 = 1.07 \times 10^{-11}$ and $[C_6H_5NO] = 4.26 \times 10^{-11}$ mol/cm^3.

The extent of our computational study is limited to the transition states TS1−TS3 immediately connected to the reactants, since the network of further transformations has been already mapped out in the earlier studies[14−16] and no experimental data on product branching are currently available for benchmarking the global $[C_9H_9]$ PES.

This article is organized as follows: In section II, we present the kinetic data on the C_6H_5 decay collected in the CRDS experiments under pseudo-first-order reaction conditions and derive the experimental total rate constant. Chemical kinetic modeling of the CRDS data is performed to further validate its interpretation in terms of pseudo-first-order reaction kinetics. Section III outlines the computational methodology used to evaluate the total and branching rate constants for the reaction of C_6H_5 with allene from first principles. Next we apply it to elucidate the mechanism and kinetics for reactions R1−R3 in section IV. In section V, we compare the rates of the C_6H_5 reactions with a series of simple unsaturated hydrocarbons and identify common trends and reactivity patterns. A brief summary concludes this article in section VI.

II. Kinetic Measurements by CRDS

Detailed descriptions of the CRDS technique for kinetic applications have been reported in our earlier publications.[8] Briefly, a heatable 50 cm long Pyrex flow tube was sealed at both ends with highly reflective mirrors ($R = 0.9999$ and radius of curvature $r = 6$ m) forming the resonance cavity which can effectively increase the lifetime of a probing laser pulse from fwhm ≈ 10 ns to 35−40 μs. The presence of absorbing species inside the cavity, however, reduces this photon decay time. The essence of the technique thus lies in measuring the variations in photon decay time in the presence of varying concentrations of the absorbing species (e.g., C_6H_5 radical) during the progress of the reaction of interest. In fact, the depletion in the reactant concentration with the progress of reaction is determined by measuring the increase in photon decay time during the reaction.

For the present study of the reaction of the C_6H_5 radical, two lasers were used for its generation and detection. The two-splitted 248-nm KrF excimer laser (Lambda Physik EMG102) beams crossing at the center of the reactor at a 30° angle were used to generate phenyl radicals from the photodissociation of nitrosobenzene. An Excimer laser (Lambda Physik EMG 201) pumped tunable dye laser (Lambda Physik FL 3002) was used to measure the decay of the C_6H_5 absorbance at 504.8 nm longitudinally through the center of the reactor. A small fraction of the probing photon pulse transmitted through the second cavity mirror was directly detected by a Hamamatsu photomultiplier tube (PMT). PMT signal was acquired and averaged by using a lock-in multichannel digital oscilloscope (LeCroy 9310M). Typically 20 pulses were collected at the rate of 2 Hz for each time delay. The averaged signal was stored in a computer for future data analysis. A pulse-delay generator (SR DG 535) interfaced with the computer using LabView software was employed to control the firing of the two lasers as well as the triggering of the data acquisition system. Allene (Aldrich, 99%) was purified by trap-to-trap distillation using appropriate slush baths. Ar carrier gas (Specialty Gases, 99.995% UHP grade) was used without further purification.

The concentration of a reagent X in the reactor ($[X]$; mol cm^{-3}) was calculated from the known molar fraction of the reagent (f_X) in its premixture with bath gas, the total pressure (P^{TOT}; Torr) and temperature (T; K) in the reactor, and controlled flow rates of each reagent's premixture (F_X) and of all gases (F^{TOT})

$$[X] = 1.603 \times 10^{-5} f_X P^{TOT} F_X / T F^{TOT} \quad \text{(I)}$$

The initial concentration of C_6H_5NO was determined by UV/vis spectrometry (SHIMADZU, UV-2401 PC) in the downstream of the reaction cell using standard calibration mixtures with $[C_6H_5NO] = (1 - 8) \times 10^{-11}$ mol cm^{-3}. The initial conversion of C_6H_5NO under normal experimental conditions is typically in the range of 5−15%.

The CRD method measures the decay times of the injected probing photons in the absence (t_c^0) and presence (t_c) of absorbing species (e.g., C_6H_5). These photon decay times can be related to the concentration of C_6H_5 at time t after its generation by the following equations:[8a−e]

$$1/t_c = 1/t_c^0 + B[C_6H_5]_0 e^{-k't} \quad \text{(IIa)}$$

or

$$\ln(1/t_c - 1/t_c^0) = C - k't \quad \text{(IIb)}$$

where $[C_6H_5]_0$ is the initial concentration of C_6H_5, B is a constant which contains experimental parameters such as the cavity length (50 cm), the refractive index of the absorbing medium, etc., $C = \ln(B[C_6H_5]_0)$, and k' is pseudo-first-order rate coefficients. Equation II is valid provided that the decay time of the species of interest is much longer than that of photons within the cavity. This condition can be readily met because the chemical decay time, typically in the range of several hundreds of microseconds to tens of milliseconds, can be controlled by the concentration of the molecular reagent.

Both first-order and second-order kinetics are illustrated in Figures 1 and 2. The slopes of the $\ln(1/t_c - 1/t_c^0)$ vs t plots illustrated in Figure 1 for the reactions of C_6H_5 with allene yield the pseudo-first-order rate coefficients, k', for the decay of C_6H_5 in the presence of known allene concentrations as specified. A standard plot of k' vs reagent concentration ($[C_3H_4]$) is shown in Figure 2, which gives the averaged second-order rate constant k_X from its slope according to the relationship

$$k' = k^0 + k_X[X] \quad \text{(III)}$$

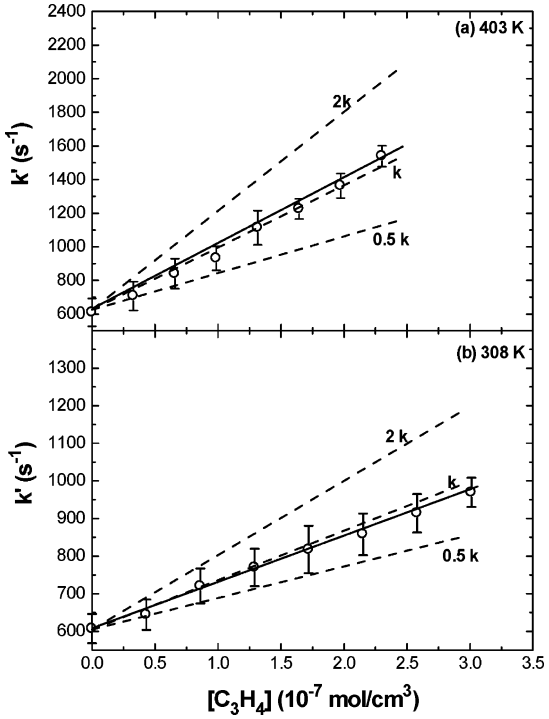

Figure 2. Typical k' vs reactant concentration plots. Solid lines are weighted least-squares fits and dashed lines are kinetically modeled results.

TABLE 1: Measured Bimolecular Rate Constants (k/10^9 cm^3 mol^{-1} s^{-1}) for the C_6H_5 Reactions with Allene

T/K	$[C_3H_4]^a$	k^b
301	0−3.52	0.92 ± 0.15
308	0−3.01	1.06 ± 0.12
325	0−2.45	1.40 ± 0.26
343	0−2.32	1.70 ± 0.23
355	0−2.61	2.03 ± 0.23
373	0−2.49	2.90 ± 0.48
403	0−2.30	3.67 ± 0.50
421	0−1.55	5.08 ± 1.07

[a] In the units of 10^{-7} mol cm^{-3}. [b] All experiments were performed at 40 Torr. The uncertainties represent 1σ, evaluated with weighted least-squares analyses by convoluting the errors in k' for k.

where k^0, shown as the y-axis intercept in Figure 2, is the radical decay constant in the absence of the molecular reactant X due to the loss of the radical by diffusion away from the probing beam and recombination reactions (e.g., reactions of C_6H_5 with NO, C_6H_5, and C_6H_5NO).

The bimolecular rate constants determined from the slopes of k' vs $[C_3H_4]$ plots are summarized in Table 1. Weighted least-squares analysis of the individual set of reaction rate constants gave rise to the following expression, in the units of cm^3 mol^{-1} s^{-1} (T = 301−421 K)

$$k_{\text{allene}} = (4.07 \pm 0.38) \times 10^{11} \exp[-(1865 \pm 85)/T]$$

The decay of C_6H_5 radicals measured in the absence of C_3H_4 in each experimental run (k^0) allows us to estimate reasonably the initial averaged concentration of C_6H_5, which in turn allows us to model k' and its dependence on the molecular reactant concentration. The detail description on kinetic modeling is given in our earlier paper.[8a] The averaged initial concentrations of phenyl radicals produced by varying photolysis laser energies in the absence of C_3H_4, modeled to be in the range of 10−50% of the initial C_6H_5NO concentration (1−8 × 10^{-11} mol cm^{-3}), decay linearly with time at small conversions (<20%) controlled mainly by the C_6H_5 + C_6H_5NO reaction, whereas they exhibit a slight nonlinear decay at higher conversions (>35%) which can be accounted for by the increasing contributions from radical−radical reactions such as C_6H_5 + C_6H_5. In current experimental conditions, the initial C_6H_5 radical concentrations were estimated in the range of 5−20% of the initial C_6H_5NO concentration. The modeled C_6H_5 decay rates using the reaction mechanism in Table 2 are shown in Figure 1 as dashed lines, representing $\ln[C_3H_4]_t - \ln[C_3H_4]_0$ vs t. Even though the C_6H_5 + C_6H_5/C_6H_5NO reactions may play a role importantly at a low-temperature range, the pseudo-first-order kinetics could be quantitatively modeled. Figure 2 also illustrates the sensitivity of the k_{allene} value to the slope in the second-order plot. Our sensitivity analysis illustrated in Figure 3 shows that the how C_6H_5 radical decay is affected by the C_6H_5 + C_3H_4 reaction. In sensitivity analysis the sensitivity coefficient is defined by $S_{ij} = (\partial C_i/\partial k_j)(k_j/C_i)$, where C_i is the concentration of the ith species and k_j is the rate constant of the jth reaction included in the mechanism.

III. Computational Methods

III.1. Quantum-Chemical Calculations. The mechanism and product branching for the C_6H_5 reaction with allene have been studied with the help of electronic structure calculations performed with the Gaussian 03[17] and MOLPRO 2002[18] program packages. Initial geometry optimizations and vibrational frequencies calculations for the reactants and transition states were performed using the hybrid gradient corrected three-parameter B3LYP density functional[19] with the 6-311++G(d,p) basis set.[20] Then minimum energy paths (MEPs) were calculated by following intrinsic reaction coordinates[21] (IRC) in steps of 5 amu$^{0.5}$ Bohr, and higher-level transition state (TS) geometries were optimized at the IRCMax-(RCCSD(T)//B3LYP) level.[10,22] Namely, a refined TS was located as the point on the MEP where the RCCSD(T)/6-311G-(d,p) energy was at its maximum.[23] RCCSD(T)[24] here denotes a partially spin-adapted open-shell coupled cluster singles and doubles theory augmented with a perturbation correction for triple excitations (MOLPRO keyword: RHF-RCCSD(T)). Projected B3LYP vibrational frequencies were calculated for the refined TSs. The calculated and available for the reactants experimental[25] molecular parameters are listed in the Supporting Information.

We used the same geometry optimization procedure in our recent studies of the C_6H_5 addition reactions to C_2H_2, C_2H_4,[10] and propyne.[11] The IRCMax approach has been also employed by Saeys et al.[26] to obtain high-level (CBS-QB3) TS geometries along the less expensive B3LYP/6-311G(d,p) reaction paths. According to these studies, the IRCMax geometries show a systematic improvement over the B3LYP data for radical addition reactions, similar to the ones studied here.

Single-point calculations using the high-level G2M[27] and G3[28] composite methods were performed to evaluate the barriers for reactions R1−R3 with chemical accuracy. The G3 method approximates the UQCISD(T,Full)/G3Large electronic energy from a series of UQCISD(T),[29] UMP4(SDTQ)[30] and UMP2 calculations with smaller basis sets. All energies are calculated using spin-unrestricted wavefunctions and a frozen core approximation, except for the UMP2(Full)/G3Large correlation calculation which includes all electrons. Among several proposed G2M-type schemes, we have selected the G2M(RCC5,-RMP2) version (eqs IV and V) on the merits of its simplicity

TABLE 2: Reactions and Rate Constants Used in the Modeling of the $C_6H_5 + C_3H_4$ Reaction in the CRD Experiment[a]

reactions	A	n	E_a	ref[b]
1a. $C_6H_5 + C_3H_4 \rightarrow C_6H_5CH_2CCH_2$	9.63×10^3	2.56	2180	this work
1b. $C_6H_5 + C_3H_4 \rightarrow CH_2(C_6H_5)CCH_2$	5.12×10^4	2.32	2920	this work
1c. $C_6H_5 + C_3H_4 \rightarrow C_6H_6 + C_3H_3$	1.87×10^0	3.68	2210	this work
2. $C_3H_3 + C_3H_3 \rightarrow C_3H_3C_3H_3$	6.00×10^{13}	0	0	*c*
3. $C_6H_5 + C_3H_3 \rightarrow C_9H_8$	4.00×10^{13}	0	0	*d*
4. $C_6H_5NO \rightarrow C_6H_5 + NO$	1.42×10^{17}	0	55060	
5. $C_6H_5 + NO \rightarrow C_6H_5NO$	2.95×10^{12}	0	-860	
6. $C_6H_5 + C_6H_5NO \rightarrow C_{12}H_{10}NO$	4.90×10^{12}	0	-68	
7. $C_6H_5 + C_6H_5 = C_{12}H_{10}$	2.39×10^{13}	0	111	
8. $C_6H_5 + C_6H_5O \rightarrow C_{12}H_{10}O$	1.00×10^{13}	0	0	
9. $C_6H_5 + C_{12}H_{10}N \rightarrow C_{18}H_{15}N$	1.00×10^{13}	0	0	
10. $C_6H_5 + C_6H_5NO \rightarrow C_{12}H_{10} + NO$	5.00×10^{12}	0	4500	
11. $C_{12}H_{10}NO + C_6H_5 \rightarrow C_{12}H_{10}N + C_6H_5O$	1.00×10^{13}	0	0	
12. $C_{12}H_{10}N + NO \rightarrow C_{12}H_{10}NNO$	1.00×10^{13}	0	0	
13. $C_{12}H_{10}NO \rightarrow C_6H_5NO + C_6H_5$	5.00×10^{14}	0	45000	

[a] Rate constants are defined by $k = AT^n \exp(-E_a/RT)$ and in units cm^3, mol, and s; E_a is in the units of cal mol^{-1}. [b] Reference 8a unless otherwise noted. [c] Reference 44. [d] Estimated from reactions 2 and 7.

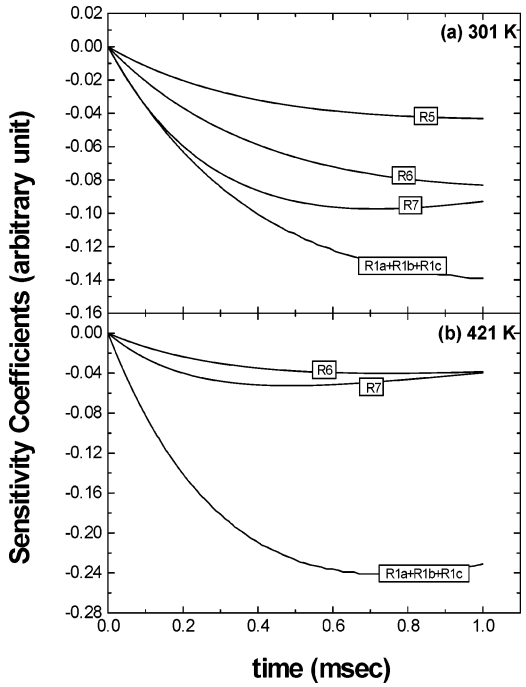

Figure 3. Sensitivity analysis for the $C_6H_5 + C_3H_4$ reaction at $P = 40$ Torr. The conditions are $[C_6H_5]_0 = 1.07 \times 10^{-11}$ mol/cm^3, $[C_6H_5NO] = 4.26 \times 10^{-11}$ mol/cm^3, $[C_3H_4] = 3.52 \times 10^{-7}$ mol/cm^3 at 301 K and $[C_6H_5]_0 = 7.62 \times 10^{-12}$ mol/cm^3, $[C_6H_5NO] = 3.05 \times 10^{-11}$ mol/cm^3, $[C_3H_4] = 1.55 \times 10^{-7}$ mol/cm^3 at 421 K. The reaction numbers are given in Table 2.

and good performance for the phenyl radical reactions with C_2H_x ($x = 2, 4$) hydrocarbons[9,10]

$$E[\text{G2M(RCC5,RMP2)}] = E[\text{RCCSD(T)/6-311G(d,p)}] + \Delta E(+3\text{df2p}) + \text{ZPE} \quad \text{(IV)}$$

$$\Delta E(+3\text{df2p}) = E[\text{RMP2/6-311+G(3df,2p)}] - E[\text{RMP2/6-311G(d,p)}] \quad \text{(V)}$$

The G2M(RCC5,RMP2) scheme exercises the use of a restricted open-shell formalism and approximates the RCCSD(T)/6-311+G(3df,2p) electronic energy in its limit. A frozen core approximation is used in the RCCSD(T)[24] and RMP2[31] calculations.

In the present implementations of the G2M and G3 methods, zero-point vibrational energy (ZPE) corrections were calculated from the unscaled B3LYP/6-311++G(d,p) vibrational frequencies and the empirical higher level corrections (HLCs) were omitted. All reactions considered in this study are isogyric (have a conserved number of electron pairs in the reactants, transition states, and products), in which case HLCs cancel out in all relative energies.

III.2. Rate Constant Calculations. The calculated molecular parameters listed in the Supporting Information were employed for the rate constant calculations by canonical transition state theory,[32] including hindered rotor treatment[33] and unsymmetric Eckart tunneling corrections,[34,35] as implemented in the ChemRate software.[36] The standard rigid rotor harmonic oscillator formalism was used to calculate vibrational and external rotational partition functions, excluding those for the low-frequency torsional modes, which were treated as free or hindered one-dimensional (1-D) internal rotations. The classical hindered rotor partition function at temperature T was calculated by the method of Pitzer and Gwinn,[33,35] assuming a sinusoidal form of the torsional potential

$$Q_{\text{hind}}(T) = \frac{(2\pi I_R kT)^{1/2}}{h} \int_0^{2\pi/i} \exp\left[-\frac{V_i(1-\cos(i\tau))}{2kT}\right] d\tau \quad \text{(VI)}$$

where I_R (kg m^2) is the reduced moment of inertia of the corresponding 1-D free rotor. Quantum effects were approximately taken into account via a multiplication of the Q_{hind} by the ratio of quantum and classical partition functions of the corresponding harmonic oscillator. The hindering barriers (V_i, kJ mol^{-1}) were estimated from the torsional frequencies (ν, cm^{-1})[35]

$$V_i \approx 8\pi^2 I_R N_A c^2 \nu^2 / i^2 \quad \text{(VII)}$$

where N_A (mol^{-1}) is the Avogadro constant, c (cm s^{-1}) is the velocity of light, and index i designates the number of minima of the torsional potential in the interval from 0 to 2π. The applicability of eq VII was tested for TS1−TS3, whose conformations (first- and second-order saddle points corresponding to the minima and maxima of the torsional potentials) were optimized with B3LYP-DFT. The V_i's estimated from eq VII were found in reasonable agreement with the values derived directly from the relative energies of different conformations.

IV. Predicted Results

IV.1. Optimized Geometries and Conformational Analysis for TS1−TS3. Optimized geometries of TS1−TS3 are shown

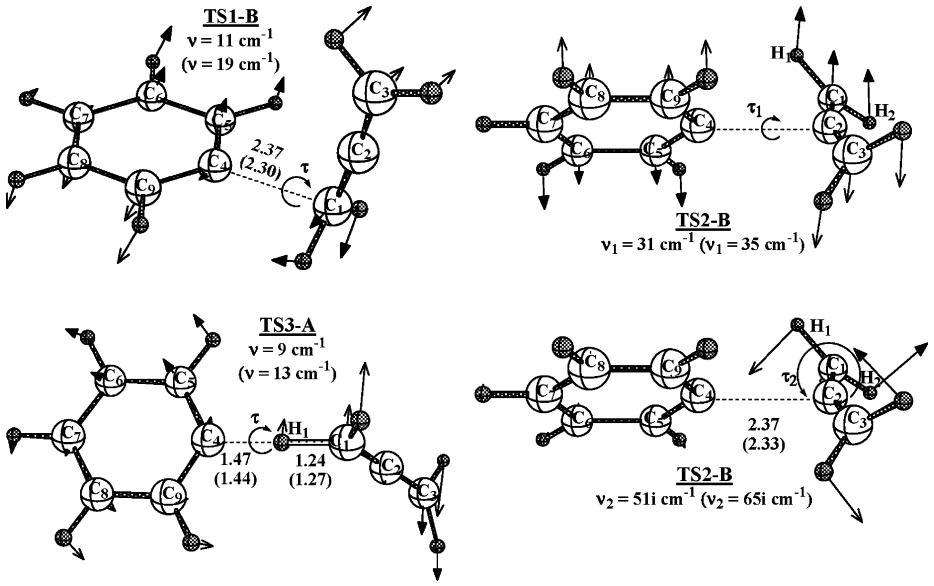

Figure 4. Optimized B3LYP and IRCMax (in parentheses) geometries (in Å) and low-barrier internal rotations of TS1−TS3. The vectors shown are proportional to the displacements calculated from the normal-mode analysis for the B3LYP-optimized structures. Torsional angles are defined in terms of dihedral angles (D): τ(TS1,TS3) = ($D_{C2C1C4C5}$ + 180° + $D_{C2C1C4C9}$)/2, τ_1(TS2) = ($D_{C1C2C4C5}$ + 180° + $D_{C1C2C4C9}$)/2, τ_2(TS2) = ($D_{C4C2C1H1}$ + 180° + $D_{C4C2C1H2}$)/2.

TABLE 3: Conformational Analysis and Estimated Torsional Barriers for TS1−TS3

	TS1			TS2				TS3	
property	**A**	**B**	**C**	**A**	**B**	**C**	**D**	**A**	**B**
symmetry	C_1	C_s	C_s	C_1	C_2	C_s	C_s	C_s	C_s
$(\tau)^a$ or $\begin{pmatrix}\tau_1\\ \tau_2\end{pmatrix}$	(58,122)	(90)	(0,180)	$\begin{pmatrix}50,130\\ 20,63,117,160\end{pmatrix}$	$\begin{pmatrix}45,135\\ 41,139\end{pmatrix}$	$\begin{pmatrix}90\\ 0,90,180\end{pmatrix}$	$\begin{pmatrix}0,180\\ 0,90,180\end{pmatrix}$	(90)	(0,180)
$E_{rel}{}^b$	0.0	0.0	0.4	0.0	0.1	0.5	3.5	0.0	0.3
V_i//B3LYP^c		$V_2 = 0.8$			$V_2 = 5.8$, $V_4 = 0.4$			$V_2 = 0.4$	
V_i//IRCMax^c		$V_2 = 2.3^{+1.0}_{-2.3}$			$V_2 = 7.5^{+1.0}_{-3.0}$, $V_4 = 0.6^{+1.0}_{-0.6}$			$V_2 = 0.9^{+1.0}_{-0.9}$	

[a] Torsional angles are defined in Figure 4. All torsional potentials have mirror symmetry about $\tau = 180°$ and $\tau = 0°$, so it suffices to list the conformations with $0 \le \tau \le 180°$. [b] E_{rel} is the energy (in kJ/mol, without ZPE correction) of a given conformation relative to the energy of the most stable conformation (**A**). [c] V_i is the torsional barrier (in kJ/mol) approximated using eq VII, given together with an assigned error range.

in Figure 4. Our B3LYP-optimized structures are virtually identical to the ones reported earlier by Vereecken et al.[14,16] The effect of geometry refinement by the higher level IRCMax method is manifested primarily in the slightly shortened transient lengths of the forming bonds.

As a consequence of their loose structure, TS1−TS3 may exhibit large amplitude motions originating from certain external rotations of the C_6H_5 and C_3H_4 fragments in the limit of infinite separation. Indeed, all TSs are flexible with respect to the internal rotation of the C_6H_5 fragment about its axis of symmetry. This motion is designated as τ or τ_1 in the TSs shown in Figure 4. We have also identified a second large amplitude transitional mode (τ_2) in TS2, which corresponds to the geared internal rotation of the CH_2 groups about the C_1-C_2 and C_2-C_3 bonds and originates from the external rotation of allene about its S_4 axis of improper rotation.

The large amplitude modes described above have been treated as hindered/free internal rotations for the purpose of partition function calculations. The hindering barriers (V_i's) were estimated from the corresponding torsional frequencies of TS1−TS3 optimized by either B3LYP-DFT or IRCMax methods. For comparison, we have also derived V_i's directly from the conformational analysis of TS1−TS3 at the B3LYP-DFT level. In the following discussion, different conformations are named alphabetically in the order of increasing total energy, beginning with the most stable form **A**. Table 3 summarizes the properties of various conformations of TS1−TS3. Figure 4 illustrates the geometries of reference conformations and provides the definitions of torsional angles.

The internal rotation of the C_6H_5 fragment in TS1//B3LYP is hindered by only 0.4 kJ/mol, an energy difference between the eclipsed TS1-**C** conformation having all C atoms in one plane ($\tau = 0°$) and the TS1-**A** ($\tau = 58°$, 122°) and TS1-**B** ($\tau = 90°$) conformations, which are virtually isoenergetic (see Table 3). The tighter TS1//IRCMax is expected to have a higher torsional barrier. Equation VII gives an estimate of V_2(TS1//IRCMax) = 2.3 kJ/mol, which is probably somewhat too high because the torsional barrier for TS1//B3LYP obtained from eq VII, V_2 = 0.8 kJ/mol, is overestimated. Taking this into account and adding an additional uncertainty of ±1 kJ/mol, we tentatively assign a range of 0 kJ/mol ≤ V_2 ≤ 3.3 kJ/mol to the C_6H_5 torsional barrier in TS1//IRCMax.

The maximum of the C_6H_5 torsional potential in TS2//B3LYP also corresponds to the eclipsed conformation (TS2-**D**, $\tau = 0°$), which lies 3.5 kJ/mol (V_2) higher in energy than the most stable conformation TS2-**A**. Equation VII overestimates the C_6H_5 torsional barrier by ~2 kJ/mol. Unlike TS1, TS2 is very flexible with respect to the geared rotation of the CH_2 groups (τ_2, Figure 4). The corresponding internal rotational profile connects the lowest energy conformations $\mathbf{A}_1$ ($\tau_2 = 20°$) and $\mathbf{A}_2$ ($\tau_2 = 63°$) via a very small barrier **B** ($\tau_2 = 41°$) and then conformations $\mathbf{A}_2$ ($\tau_2 = 63°$) and $\mathbf{A}_3$ ($\tau_2 = 117°$) via a slightly higher barrier

TABLE 4: Theoretical Barriers (0 K, in kJ/mol) for Reactions of Phenyl Radicals with Allene (R1−R3), Methane (R4),[a] Ethylene (R5),[b] and Acetylene (R6)[c]

	calculated reaction barriers					
methods	TS1	TS2	TS3	TS4	TS5	TS6
B3LYP/6-311++G(d,p) Optimization						
B3LYP/6-311++G(d,p)	17.1	27.3	15.0	33.6	13.8	18.5
RMP2/6-311G(d,p)	11.3	13.0	17.4	26.8	9.4	13.7
RCCSD(T)/6-31G(d,p)	14.9	17.0	27.9	47.2	11.9	16.4
RCCSD(T)/6-311G(d,p)	14.5	17.1	24.5	41.5	11.7	18.3
UCCSD(T)/6-311G(d,p)	14.5[d]	17.9[d]	24.5[d]	41.7	11.9	19.0
G2M(RCC5,RMP2)	11.5	13.6	21.4	38.5	8.6	15.5
IRCMax(RCCSD(T)//B3LYP) Optimization						
G3	8.6	14.1	16.7		7.2	12.9
G2M(RCC5,RMP2)	11.9	13.9	21.8		9.5	15.7

[a] From refs 37 and 38. [b] From ref 10. [c] From refs 9 and 10. [d] From ref 16; geometries were optimized by the B3LYP/6-311+G(d,p) method.

C ($\tau_2 = 90°$). The $V(\tau_2)$ hindering potential has mirror symmetry about $\tau_2 = 0°$, 90° and 180°, so it can be approximated by a sinusoidal potential with V_4(TS2//B3LYP) = 0.5 kJ/mol. A very similar estimate of V_4(TS2//B3LYP) = 0.4 kJ/mol is given by eq VII. For the IRCMax optimized geometry of TS2, we estimate that 4.5 kJ/mol $\leq V_2 \leq$ 8.5 kJ/mol and $V_4 \leq$ 1.6 kJ/mol.

The calculated torsional frequencies for TS3 are extremely low, and the corresponding torsional potential is virtually flat which allows for an essentially free internal rotation of the phenyl group in TS3. With an added uncertainty, we estimate that V_2(TS3//IRCMax) $\leq$ 1.9 kJ/mol. The final estimates of the internal rotational barriers for TS1−TS3 and the assigned error ranges are summarized in Table 3.

IV.2. Barriers for Reactions R1−R3. The barriers for reactions R1−R3 were evaluated from higher level single-point calculations, using the B3LYP and IRCMax geometries of the low energy conformations of TS1−TS3 shown in Figure 4. The lowest energy **A** conformations were selected for TS3. For TS1 and TS2, the symmetric **B** conformations were favored, because they are virtually isoenergetic (within 0.1 kJ/mol) with the unsymmetric **A** conformations, but the cost of high-level electronic structure computations could be significantly reduced by taking advantage of molecular symmetry.

Table 4 lists the 0 K barriers for reactions R1−R3 calculated in this work and in the study of Vereecken and Peeters.[16] For comparison, we have also included in Table 4 our calculated barriers for the prototypical reactions of C_6H_5 with CH_4,[37,38] C_2H_2,[9,10] and C_2H_4[10]

$$C_6H_5 + CH_4 \xrightarrow{TS4} C_6H_6 + CH_3 \qquad (R4)$$

$$C_6H_5 + C_2H_4 \xrightarrow{TS5} C_6H_5CH_2CH_2 + CH_3 \qquad (R5)$$

$$C_6H_5 + C_2H_2 \xrightarrow{TS6} C_6H_5CHCH \qquad (R6)$$

Common trends can be found from an examination of the theoretical barriers for analogous reactions, such as the H-transfer reactions (R3 and R4) and the C_6H_5-addition reactions to the sp^2 carbon (R1 and R5) or to the sp carbon (R2 and R6). For example, the B3LYP-DFT tends to underestimate the H-abstraction barriers and overestimates the barriers for the examined C_6H_5 addition reactions. As a result, this method predicts qualitatively incorrect barriers for the branching channels (R1−R3). At the higher levels of theory (e.g., (R/U)CCSD-(T), G2M, G3), the C_6H_5 addition to the terminal carbon atom in allene is consistently found to be the most energetically favorable reaction channel. Of particular concern to us, however, is the quantitative accuracy of the theoretical predictions.

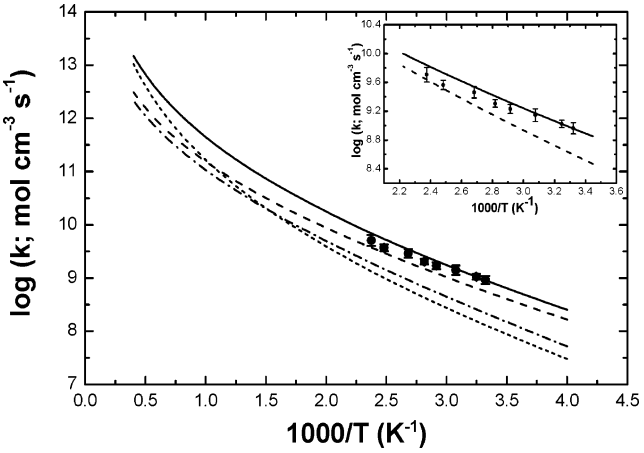

Figure 5. Calculated (lines) and experimental (filled squares with error bars) rate constants for the C_6H_5 reaction with allene. The experimental values are measured in this work by CRDS. The main plot shows k_{allene} (solid line), k_{R1} (dashed line), k_{R2} (dot-dashed line), and k_{R3} (dotted line) calculated in this work at the G2M//IRCMax level. The inset also shows predicted k_{allene} from this work (solid line) and from the study of Vereecken et al.[16] (dashed line) at the UCCSD(T)/6-311G(d,p)//B3LYP-DFT level of theory.

In our experience, ab initio methods that employ a spin-unrestricted single-reference wavefunction may not predict reliable energetic parameters for reactions involving aromatic and delocalized radicals, because these methods are prone to severe spin-contamination problems. For the present C_9H_9 system, we observe a slow convergence of the UMPn series and a poor performance of the UMP2 and UMP4 methods (listed in the Supporting Information). However, we find that restricted and unrestricted CCSD(T)/6-311G(d,p) barriers are very similar for all reactions included in Table 3, which indicates that the CCSD(T) treatment of electron correlation cures the spin contamination problem. When combined with sufficiently large basis sets, this method's predictions should be of chemical accuracy or better. The basis set extension correction (eq 5) added in the G2M(RCC,RMP2) composite scheme lowers the RCCSD(T)/6-311G(d,p) barriers by ∼2−4 kJ/mol. The G3 barriers are further ∼2−5 kJ/mol below the G2M values, except for the $E_0°$(R2), which both methods closely agree upon. As alluded to above, G3 theory uses spin-unrestricted formalism in the calculation of its UQCISD(T), UMP4, and UMP2 energy components, which suffer from adverse effects of spin contamination. Although most of the associated errors are expected to cancel out in the G3 composite energy, we believe that the G2M(RCC,RMP2) method provides more reliable estimates of the barriers listed in Table 4.

Previously, we found the G2M(RCC,RMP2) energetic parameters for reactions R4−R6 in good agreement with available benchmark values.[9,10,38] In particular, the G2M(RCC,RMP2) barriers have been used without any adjustments[9,10] to account for the available kinetic data for reactions (R5) and (R6). Our best estimate of $E_0°$(R4) = 38.5 kJ/mol agrees well with the values of 37.9 kJ/mol recently obtained at the W1 level of theory[39] and 43.9 kJ/mol used to fit the measured rate constants for reaction (R4).[37] Taking into account good performance of the G2M(RCC,RMP2) method for reactions R4−R6, we expect the predicted barriers for analogous reactions R1−R3 to be of chemical accuracy as well (±5 kJ/mol).

IV.3. Total Rate Constant and Initial Product Branching. The experimental total rate constant for the C_6H_5 reaction with allene (k_{allene}) determined in this work can be used to benchmark the theoretical predictions. As follows from the RRKM/master equation analysis of Vereecken et al.,[16] collisional stabilization of the chemically activated radicals **1** and **2** under the conditions of our CRDS measurements (P = 40 Torr, T < 430 K) is sufficiently rapid for the rates of the C_6H_5 addition reactions (R1 and R2) to be at the high-pressure limit. Minor changes in the reaction barriers and enthalpies are not expected to shift the k_{R1} and k_{R2} rate constants far into the falloff regime. Then the total rate constant for the C_6H_5 reaction with allene can be estimated as a sum of the initial branching rate constants calculated by transition state theory: $k_{allene} = k_{R1} + k_{R2} + k_{R3}$. The total and branching rate constants calculated from the G2M(RCC,RMP2) energetic and IRCMax molecular parameters (listed in Tables 3 and 4 and in the Supporting Information) can be given by the following expressions, in units of $cm^3\ mol^{-1}\ s^{-1}$ (T = 250−2500 K)

$$k_{allene} = 3.27 \times 10^2\ T^{3.19} \exp[-1014/T]$$

$$k_{R1} = 9.63 \times 10^3\ T^{2.56} \exp[-1096/T]$$

$$k_{R2} = 5.12 \times 10^4\ T^{2.32} \exp[-1470/T]$$

$$k_{R3} = 1.87\ T^{3.81} \exp[-1110/T].$$

The rate constants for the reaction of C_6H_5 with allene are plotted in Figure 5. The experimental values of k_{allene} agree very well (within 40%) with the G2M//IRCMax theoretical curve without any empirical adjustments. The rate constants reported earlier by Vereecken et al.[16] were calculated from the UCCSD(T)/6-311G(d,p) energetic and B3LYP-DFT molecular parameters. Their k_{allene} is slightly lower than the experimental values by up to a factor of 2.3. Considering the uncertainties in the theoretical barriers (±5 kJ/mol) the observed agreement of the theoretical and experimental total rate constants is remarkably good. Additional sources of theoretical uncertainties lie in the approximate treatment of hindered rotations in TS1−TS3 and the tunneling effect. However, the associated errors in the calculated total rate constant are expected to be relatively small.[11]

Our calculations predict that the C_6H_5 addition at the terminal C atoms in allene (R1) is the most kinetically favorable reaction channel under the conditions of our CRDS experiments. At room T, the branching ratios are k_{R1}:k_{R2}:k_{R3} ∼ 4.7:1.8:1.0. However, the H-abstraction channel (R3) becomes more competitive at higher T and dominates the product distribution in the high T regime (T > 800 K). Qualitatively similar predictions of the product branching for the reaction of C_6H_5 with allene have been obtained in the earlier theoretical investigations by Vereecken et al.[16]

The kinetic preference of the terminal addition at low temperatures formally contradicts the Hammond's rule that predicts a lower barrier for the C_6H_5 addition at the central C atom, producing the more stable $C_6H_5C(CH_2)_2$ radical. A closer examination of the reaction path for the central addition reveals that the formation of the $C_6H_5-C(CH_2)_2$ bond is coupled with the rotation of the CH_2 groups into the C_6H_5 plane. In the ground electronic state of allene, the transition state for internal rotation of the CH_2 groups has C_{2v} symmetry and is a planar bent open-shell singlet ($^1A_2$),[40] with the barrier to planarity of ∼190 kJ/mol. This structural rearrangement is unfavorable in the early stages of the central addition, where TS2 is located (see Figure 4). As the reaction progresses, the overlap between the π orbitals of the C_6H_5 and C_3H_4 fragments becomes more efficient which leads to the resonant stabilization of the planar $C_6H_5C(CH_2)_2$ radical, where the unpaired electron is delocalized over the whole π system. On the other hand, the unpaired electron in $C_6H_5CH_2CHCH_2$ is localized on the β-C atom of the side chain and this radical is not stabilized by resonance effects. However, despite the higher product stability, the barrier for central addition (TS2) is higher than that for terminal addition (TS1), because the former channel requires greater structural changes of the C_3H_4 fragment, which are not compensated by the resonance stabilization effects in the early reaction stages.

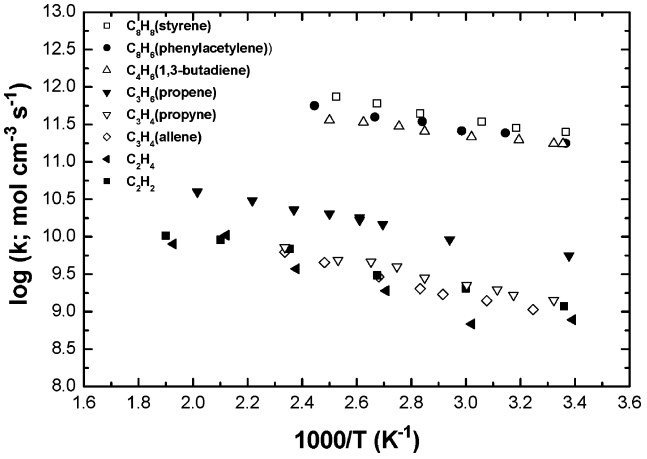

Figure 6. Comparison of reaction rates of the C_6H_5 with several unsaturated hydrocarbons; C_2H_2 (acetylene), C_2H_4 (ethylene), CH_2CO (ketene), a-C_3H_4 (allene), p-C_3H_4 (propyne), C_3H_6 (propene), C_4H_6 (1,3-butadiene), C_8H_6 (phenylacetylene), and C_8H_8 (styrene).

V. Reactivity of Unsaturated Hydrocarbons in the Addition Reactions with C_6H_5

Over the past years, we have collected experimental and theoretical kinetic data for a series of the C_6H_5 reactions with simple unsaturated hydrocarbons. Figure 6 summarizes our measured rate constants for the reactions of C_6H_5 with ethylene (C_2H_4),[8n] acetylene (C_2H_2),[41] allene (a-C_3H_4), propyne (p-C_3H_4),[11] propene (C_3H_6),[12] butadiene (1,3-C_4H_6),[42] phenylacetylene (C_8H_6), and styrene (C_8H_8).[43] The barriers and initial product branching for the C_6H_5 reactions with C_2H_2, C_2H_4, a-C_3H_4, p-C_3H_4, and C_3H_6 have been also evaluated theoretically with the help of the electronic structure calculations at the G2M level of theory; lower-level calculations have been carried out for the reactions of C_6H_5 with 1,3-C_4H_6, C_8H_6, and C_8H_8. These results can be used to infer common reactivity patterns and substitution effects. Here, we will briefly discuss some of the observed qualitative trends; the quantitative structure−reactivity correlations will be deferred to a future systematic study.

From the comparison of the experimental rate constants shown in Figure 6, the following reactivity scale can be deduced for various substrates reacting with C_6H_5 at $T \approx 300 - 400$ K: $C_2H_4 \sim C_2H_2 \sim$ a-$C_3H_4 \sim$ p-$C_3H_4 <$ $C_3H_6 <$ 1,3-$C_4H_6 <$ $C_8H_6 <$ C_8H_8. According to our theoretical predictions, the C_6H_5-additions to the terminal sp^2 or sp-hybridized C atoms are expected to be the dominant channels for all considered reactions under the conditions of our CRDS measurements (T = 301 − 421 K). Substitution of the H atom with an electron-donating CH_3 group generally increases the reactivity of the unsaturated CC bonds toward radical addition, which is consistent with the

higher measured k_{p-C3H4} and k_{C3H6} compared to k_{C2H2} and k_{C2H4}, respectively. Phenylacetylene, styrene, and 1,3-butadiene contain delocalized resonant π-electronic systems, which make the terminal sp- and sp^2-C atoms in these molecules much more reactive compared to the sp- and sp^2-C centers in C_2H_2 and C_2H_4, respectively. Not surprisingly, the measured k_{C4H6}, k_{C8H6}, and k_{C8H8} are much higher than other rate constants plotted in Figure 6.

The measured rate constants for the C_6H_5-addition to C_2H_2, C_2H_4, a-C_3H_4, and p-C_3H_4 are similar to each other (within the experimental scatter). We found that the relative magnitude of the theoretical rate constants for these reactions is determined by a delicate balance between the enthalpic and entropic factors. The standard activation enthalpies ($\Delta H^{\ddagger}_{298}$, kJ mol^{-1}, evaluated at the G2M//IRCMax level) for the C_6H_5-addition to the sp- and sp^2-C centers in various substrates increase in the following order: $\mathbf{C}_2H_4$ (8.1), $\mathbf{C}H_2C\mathbf{C}H_2$ (10.8), $CH_3C\mathbf{C}H$ (12.2), $CH_2\mathbf{C}CH_2$ (13.4), $\mathbf{C}_2H_2$ (14.1), and $CH_3\mathbf{C}CH$ (16.6). Since the differences in activation enthalpies in most of these cases are not very large, activation entropies play an important role in determining the relative rates. The standard entropies of activation ($\Delta S^{\ddagger}_{298}$, J mol^{-1} K^{-1}) for the same reactions change in a different order: $\mathbf{C}_2H_2$ (−113), $CH_3C\mathbf{C}H$ (−120), $CH_3\mathbf{C}CH$ (−125), $\mathbf{C}H_2C\mathbf{C}H_2$ (−126), $CH_2\mathbf{C}CH_2$ (−126), and $\mathbf{C}_2H_4$ (−129). The less negative (and more favorable) entropies of activation are predicted for the C_6H_5 additions to the terminal sp-C atoms. This factor is responsible for a slightly higher reactivity of p-C_3H_4 compared to a-C_3H_4 at $T > 300$ K. At higher temperatures relevant to the combustion conditions ($T > 1000$ K), C_2H_2 is expected to become more reactive toward the C_6H_5-addition than C_2H_4 and C_3H_4 isomers due to a more favorable entropy component.

VI. Conclusions

Reaction of the phenyl radical with allene has been investigated experimentally and theoretically. The total rate constant measured by the CRDS technique can be expressed by the following Arrhenius equation: $k_{allene}(301 - 421\ \mathrm{K}) = (4.07 \pm 0.38) \times 10^{11} \exp[-(1865 \pm 85)/T]$ cm^3 mol^{-1} s^{-1}. Theoretical kinetic calculations provide additional insights into reaction mechanisms and allow to evaluate the initial product branching. Under our experimental conditions, phenyl radicals preferably add to the terminal carbon atoms in allene forming 3-phenylpropen-2-yl [**1**] radicals. At higher T, the H-abstraction channel R3, forming benzene and propargyl radical, is predicted to become more important. These predictions are qualitatively similar to the results of the earlier theoretical investigations by Vereecken et al.[16] The total rate constants calculated in this work using high level G2M//IRCMax(RCCSD(T)//B3LYP-DFT) energetic and molecular parameters agree with the experimental values within 40%. The modified Arrhenius expressions of the predicted total and branching rate constants at the high-pressure limit are provided for high T applications. Our previous and present studies provide theoretical and experimental kinetic data for a series of the phenyl radical reactions with small unsaturated hydrocarbons which can be used to derive quantitative structure−reactivity correlations. Such correlations could provide valuable kinetic parameters for the reactions of more complex aryl radicals with various unsaturated hydrocarbons which will be the subject of our future work.

Acknowledgment. The authors are grateful for the support of this work from the Department of Energy, Office of Basic Energy Sciences, Division of Chemical Sciences through Contract DE-FGO2-97ER14784. Also, we are thankful to the Cherry L. Emerson Center of Emory University for the use of its resources, which is in part supported by National Science Foundation Grant CHE-0079627 and an IBM Shared University Research Award.

Supporting Information Available: Tables S1, S2, and S3 contain the geometries and molecular parameters for all species and transition states calculated in this study. Tables S4 and S5 contain detailed energetics calculated at various theoretical levels. This material is available free of charge via the Internet at http://pubs.acs.org.

References and Notes

(1) Frenklach, M. *Phys. Chem. Chem. Phys*. **2002**, *4*, 2028−2037.
(2) Richter, H.; Howard, J. B. *Prog. Energy Combust. Sci*. **2000**, *26*, 565−608.
(3) Richter, H.; Howard, J. B. *Phys. Chem. Chem. Phys*. **2002**, *4*, 2038−2055.
(4) Miller, J. A.; Pilling, M. J.; Troe, J. *Proc. Combust. Inst*. **2005**, *30*, 43−88.
(5) Frenklach, M.; Feigelson, E. D. *Astrophys. J*. **1989**, *341*, 372.
(6) Kaiser, R. I. *Chem. Rev*. **2002**, *102*, 1309.
(7) Kaiser, R. I.; Vereecken, L.; Peeters, J.; Bettinger, H. F.; Schleyer, P. v. R.; Schaefer, H. F., III. *Astron. Astrophys*. **2003**, *406*, 385.
(8) (a) Choi, Y. M.; Park, J.; Lin, M. C. *ChemPhysChem*, **2004**, *5*, 661. (b) Choi, Y. M.; Park, J.; Lin, M. C. *J. Phys. Chem. A* **2003**, *107*, 7755. (c) Choi, Y. M.; Xia, W. S.; Park, J.; Lin, M. C. *J. Phys. Chem. A* **2000**, *104*, 7030. (d) Park, J.; Burova, S.; Rodgers, A. S.; Lin, M. C. *J. Phys. Chem. A* **1999**, *103*, 9036. (e) Park, J.; Lin, M. C. *ACS Symp. Ser*. **1999**, *720*, 196. (f) Park, J.; Gheyas, S.; Lin, M. C. *Int. J. Chem. Kinet*. **1999**, *31*, 645. (g) Park, J.; Chakraborty, D.; Bhusari, D. M.; Lin, M. C. *J. Phys. Chem. A* **1999**, *103*, 4002. (h) Yu, T.; Lin, M. C. *J. Am. Chem. Soc*. **1993**, *115*, 4371. (i) Yu, T.; Lin, M. C. *J. Phys. Chem*. **1995**, *99*, 8599. (j) Yu, T.; Lin, M. C. *J. Phys. Chem*. **1994**, *98*, 9697. (k) Yu, T.; Lin, M. C. *J. Phys. Chem*. **1994**, *98*, 2105. (l) Yu, T.; Lin, M. C. *J. Am. Chem. Soc*. **1994**, *116*, 9571. (m) Diau, E. W.; Yu, T.; Wagner, M. A. G.; Lin, M. C. *J. Phys. Chem*. **1994**, *98*, 4034. (n) Yu, T.; Lin, M. C. *Combust. Flame* **1995**, *100*, 169. (o) Yu, T.; Lin, M. C. *Int. J. Chem. Kinet*. **1994**, *26*, 771. (p) Lin, M. C.; Yu, T. *Int. J. Chem. Kinet*. **1993**, *25*, 875. (q) Nam, G.-J.; Xia, W.; Park, J.; Lin, M. C. *J. Phys. Chem. A* **2000**, *104*, 1233.
(9) Tokmakov, I. V.; Lin, M. C. *J. Am. Chem. Soc*. **2003**, *125*, 11397.
(10) Tokmakov, I. V.; Lin, M. C. *J. Phys. Chem. A* **2004**, *108*, 9697.
(11) Tokmakov, I. V.; Park, J.; Lin, M. C. *ChemPhysChem* **2005**, *6* (10), 2075.
(12) Park, J.; Nam, G.; Tokmakov, I. V.; Lin, M. C. *J. Phys. Chem. A* **2006**, *110*, 8729.
(13) Radicals **1** and **2** have cis-trans isomers, which can easily interchange (see ref 14). For the purposes of this study, they are considered indistinguishable.
(14) Vereecken, L.; Peeters, J.; Bettinger, H. F.; Kaiser, R. I.; Schleyer, P. v. P.; Schaefer, H. F., III. *J. Am. Chem. Soc*. **2002**, *124*, 2781.
(15) Vereecken, L.; Bettinger, H. F.; Peeters, J. *Phys. Chem. Chem. Phys*. **2002**, *4*, 2019.
(16) Vereecken, L.; Peeters, J. *Phys. Chem. Chem. Phys*. **2003**, *5*, 2807.
(17) Frisch, M. J.; Trucks, G. W.; Schlegel, H. B.; Scuseria, G. E.; Robb, M. A.; Cheeseman, J. R.; Montgomery, J. A., Jr.; Vreven, T.; Kudin, K. N.; Burant, J. C.; Millam, J. M.; Iyengar, S. S.; Tomasi, J.; Barone, V.; Mennucci, B.; Cossi, M.; Scalmani, G.; Rega, N.; Petersson, G. A.; Nakatsuji, H.; Hada, M.; Ehara, M.; Toyota, K.; Fukuda, R.; Hasegawa, J.; Ishida, M.; Nakajima, T.; Honda, Y.; Kitao, O.; Nakai, H.; Klene, M.; Li, X.; Knox, J. E.; Hratchian, H. P.; Cross, J. B.; Bakken, V.; Adamo, C.; Jaramillo, J.; Gomperts, R.; Stratmann, R. E.; Yazyev, O.; Austin, A. J.; Cammi, R.; Pomelli, C.; Ochterski, J. W.; Ayala, P. Y.; Morokuma, K.; Voth, G. A.; Salvador, P.; Dannenberg, J. J.; Zakrzewski, V. G.; Dapprich, S.; Daniels, A. D.; Strain, M. C.; Farkas, O.; Malick, D. K.; Rabuck, A. D.; Raghavachari, K.; Foresman, J. B.; Ortiz, J. V.; Cui, Q.; Baboul, A. G.; Clifford, S.; Cioslowski, J.; Stefanov, B. B.; Liu, G.; Liashenko, A.; Piskorz, P.; Komaromi, I.; Martin, R. L.; Fox, D. J.; Keith, T.; Al-Laham, M. A.; Peng, C. Y.; Nanayakkara, A.; Challacombe, M.; Gill, P. M. W.; Johnson, B.; Chen, W.; Wong, M. W.; Gonzalez, C.; Pople, J. A. *Gaussian 03*, revision C.1; Gaussian, Inc.: Wallingford, CT, 2004.
(18) Amos, R. D.; Bernhardsson, A.; Berning, A.; Celani, P.; Cooper, D. L.; Deegan, M. J. O.; Dobbyn, A. J.; Eckert, F.; Hampel, C.; Hetzer, G.; Knowles, P. J.; Korona, T.; Lindh, R.; Lloyd, A. W.; McNicholas, S. J.; Manby, F. R.; Meyer, W.; Mura, M. E.; Nicklass, A.; Palmieri, P.; Pitzer, R.; Rauhut, G.; Schütz, M.; Schumann, U.; Stoll, H.; Stone, A. J.; Tarroni, R.; Thorsteinsson, T.; Werner, H.-J. *MOLPRO*, version 2002.6.; University of Birmingham: Birmingham, U.K., 2003.

(19) (a) Becke, A. D. *J. Chem. Phys*. **1993**, *98*, 5648. (b) Becke, A. D. *Phys. Rev. A* **1988**, *38*, 3098. (c) Lee, C.; Yang, W.; Parr, R. G. *Phys. Rev. B* **1988**, *37*, 785. (d) Stephens, P. J.; Devlin, F. J.; Chabalowski, C. F.; Frisch, M. J. *J. Phys. Chem*. **1994**, *98*, 11623.

(20) Pople, J. A.; Head-Gordon, M.; Raghavachari, K. *J. Chem. Phys*. **1987**, *87*, 5968.

(21) (a) Gonzalez, C.; Schlegel, H. B. *J. Chem. Phys*. **1989**, *90*, 2154−2161. (b) Gonzalez, C.; Schlegel, H. B. *J. Phys. Chem*. **1990**, *94*, 5523−5527.

(22) Malick, D. K.; Petersson, G. A.; Montgomery, J. A., Jr. *J. Chem. Phys.* **1998**, *108*, 5704 and references therein.

(23) This procedure is analogous to the IRCMax calculation in *Gaussian 03*, except here the higher-level single point energy calculations were carried out in *MOLPRO* 2002.

(24) (a) Knowles, P. J.; Hampel, C.; Werner, H. J. *J. Chem. Phys*. **1993**, *99*, 5219−5227 and references therein (b) Knowles, P. J.; Hampel, C.; Werner, H. J. *J. Chem. Phys*. **2000**, *112*, 3106−7. (c) Watts, J. D.; Gauss, J.; Bartlett, R. J. *J. Chem. Phys*. **1993**, *98*, 8718.

(25) *Computational Chemistry Comparison and Benchmark Database*, NIST Standard Reference Database Number 101; Johnson, R. D., III, Ed.; National Institute of Standards and Technology: Gaithersburg, MD, 2003; http://srdata.nist.gov/cccbdb/.

(26) Saeys, M.; Reyniers, M.-F.; Marin, G. B.; Van Speybroeck, V.; Waroquier, M. *J. Phys. Chem. A* **2003**, *107*, 9147.

(27) Mebel, A. M.; Morokuma, K.; Lin, M. C. *J. Chem. Phys*. **1995**, *103*, 7414.

(28) G3 theory was first introduced in Curtiss, L. A.; Raghavachari, K.; Redfern, P. C.; Rassolov, V.; Pople, J. A. *J. Chem. Phys*. **1998**, *109*, 7764. G3//B3LYP and G3X versions using B3LYP-DFT for geometry optimization were proposed later in Baboul, A. G.; Curtiss, L. A.; Redfern, P. C.; Raghavachari, K. *J. Chem. Phys*. **1999**, *110*, 7650. Curtiss, L. A.; Redfern, P. C.; Raghavachari, K.; Pople, J. A. *J. Chem. Phys*. **2001**, *114*, 108.

(29) (a) Pople, J. A.; Head-Gordon, M.; Raghavachari, K. *J. Chem. Phys.* **1987**, *87*, 5968. (b) Gauss, J.; Cremer, C. *Chem. Phys. Lett*. **1988**, *150*, 280. (c) Salter, E. A.; Trucks, G. W.; Bartlett, R. J. *J. Chem. Phys*. **1989**, *90*, 1752.

(30) (a) Krishnan, R.; Pople, J. A. *Int. J. Quant. Chem.* **1978**, *14*, 91. (b) Krishnan, R.; Frisch, M. J.; Pople, J. A. *J. Chem. Phys.* **1980**, *72*, 4244.

(31) RMP2 is a restricted open-shell MP2 (Gaussian keyword: ROMP2) described in Knowles, P. J.; Andrews, J. S.; Amos, R. D.; Handy, N. C.; Pople, J. A *Chem. Phys. Lett*. **1991**, *186*, 130.

(32) Laidler, K. J. *Chemical Kinetics*, 3rd ed.; Harper and Row: New York, 1987.

(33) Pitzer, K. S.; Gwinn, W. D. *J. Chem. Phys*. **1942**, *10*, 428−440.

(34) Eckart, C. *Phys. Rev*. **1930**, *35*, 1303.

(35) Forst, W. *Unimolecular Reactions: A Concise Introduction*; Cambridge University Press: New York, 2003.

(36) Mokrushin, V.; Bedanov, V.; Tsang, W.; Zachariah, M.; Knyazev, V. *ChemRate*, version 1.19.; NIST: Gaithersburg, MD, 2002.

(37) Tokmakov, I. V.; Park, J.; Gheyas, S.; Lin, M. C. *J. Phys. Chem. A* **1999**, *103*, 3636.

(38) Tokmakov, I. V. *Computational studies of reactions responsible for the formation and removal of phenyl radicals in hydrocarbon combustion*; Emory University: Atlanta, GA 2003.

(39) Hemelsoet, K.; Moran, D.; Van Speybroeck, V.; Waroquier, M.; Radom, L. *J. Phys. Chem. A* **2006**, *110*, 8942.

(40) Bettinger, H. F.; Schreiner, P. R.; Schleyer, P. v. R.; Schaefer, H. F., III. *J. Phys. Chem.* **1996**, *100*, 16147.

(41) Yu, T.; Lin, M. C.; Melius, C. F. *Int. J. Chem. Kinet.* **1994**, *26*, 1095.

(42) Ismail, Huzeifa.; Park, J.; Wonga, Bryan M.; Green, W. H. Jr.; Lin, M. C. *Proc. Combust. Inst.* **2005**, *30*, 1049−1056.

(43) Nam, G.; Tokmakov, I. V.; Park J.; Lin, M. C. *Proc. Combust. Inst.* **2007**, *31*, 249−256.

(44) The NIST Chemical Kinetics Database, 17-2Q98, 1998.